LAWRENCE
LIVERMORE
NATIONAL
LABORATORY

LLNL-TR-765862

Fission Gamma-Ray Spectra Relevant to Post-Detonation Debris Analysis

A. Tonchev, J. Silano, J. Wilhelmy, M. Gooden

January 16, 2019

Disclaimer

This document was prepared as an account of work sponsored by an agency of the United States government. Neither the United States government nor Lawrence Livermore National Security, LLC, nor any of their employees makes any warranty, expressed or implied, or assumes any legal liability or responsibility for the accuracy, completeness, or usefulness of any information, apparatus, product, or process disclosed, or represents that its use would not infringe privately owned rights. Reference herein to any specific commercial product, process, or service by trade name, trademark, manufacturer, or otherwise does not necessarily constitute or imply its endorsement, recommendation, or favoring by the United States government or Lawrence Livermore National Security, LLC. The views and opinions of authors expressed herein do not necessarily state or reflect those of the United States government or Lawrence Livermore National Security, LLC, and shall not be used for advertising or product endorsement purposes.

This work performed under the auspices of the U.S. Department of Energy by Lawrence Livermore National Laboratory under Contract DE-AC52-07NA27344.

Fission Gamma-Ray Spectra Relevant to Post-Detonation Debris Analysis

Anton P. Tonchev, Jack Silano
LLNL

Jerry Wilhelmy, Matthew Gooden
LANL

Abstract

A terrorist-generated nuclear attack would invoke unprecedented pressure for a rapid and accurate nuclear forensics characterization of the event. In-situ fission product gamma-ray spectroscopy offers the potential for a significant reduction in analysis time while still providing high fidelity identification of the primary composition of the detonated device. The *in-situ* spectroscopic approach we are proposing can rapidly identify the species that underwent fission as well as the fission-inducing neutron energy spectrum. To demonstrate this goal, we have used the gamma-ray history from our previously obtained LLNL-LANL-TUNL fission product-yield (FPY) data to provide insights for post-detonation debris analysis. The proposed method relies on the ratio of photopeak areas for selected gamma-rays representing the FPYs of sixteen fission products generated using mono-energetic neutrons at energies between 0.5 MeV to 14.8 MeV on highly-enriched ^{239}Pu,^{235}U, and ^{238}U sealed targets. In addition to the fission product ratio measurements we have applied a new regression analysis based on our experimental FPY data and validated the approach using relevant Godiva FPY data and (surrogate) photofission product yields of ^{240}Pu. The main advantage of the regression analysis is that it investigates the FPY data set as a whole, rather than focusing on individual FPY ratios.

I. Introduction

When a nucleus undergoes fission, the products emit both prompt and delayed characteristic γ-rays. The delayed γ-rays can be used to identify fissionable material in post-detonation debris. In the aftermath of an above ground nuclear explosion, measuring the isotopic compositions of fallout can provide important forensic information, including data pertaining to the production and irradiation histories of key materials. Quantifying the fissile content from trace amounts of nuclear material is of significant importance to the safeguards and nuclear forensics communities. Though radiochemical methods remain central to fission-yield measurements, there is a growing need in nuclear safeguard applications for alternative techniques that are much more rapid and do not damage or destroy the radioactive sample. However, despite the multi decade accumulation of fission-yield measurements, whether by gamma rays or other means, there is a continuing demand

for additional high quality measurements and data evaluations more centric to the nuclear forensic mission.

Current responders can measure the individual FPYs by one of the following three methods: 1) direct (instrumental) high-resolution gamma-ray spectrometry of the sample, 2) radiochemical separation of the fission products followed by beta or gamma-ray counting, and 3) mass spectrometry. The purpose of sampling the debris produced as a result of a nuclear explosion is to provide material for radiochemical analysis of products of the explosion. Subsequent interpretation of the radiochemical analysis results provides insight into the type of fuel, the physical makeup, the operational efficiency, and the level of technological sophistication of the detonated device. Table 1 lists the main advantages and disadvantages for isotope assay. Traditional approaches have relied on destructive analysis measurements or passive detection of gamma/neutron signatures through nondestructive assay. These methods can be highly accurate and employed globally as both a nuclear forensics capability and for material accountability measurements. However, common destructive-analysis techniques rely on sample dissolution, a time-consuming process which can be particularly difficult for certain sample matrices, such as melt-glass formed from nuclear fallout. Similarly, trace quantities of nuclear materials prove difficult to measure using passive nondestructive assay techniques due to relatively low emission rates and potential interference from activated materials within the sample matrix. Additionally, the timeliness of fissile material assay is of concern for both treaty verification and post-nuclear detonation scenarios.

Table 1. The main experimental techniques used for isotope assay analysis.

Method	Precision	Expeditiousness	Target mass
Mass spectrometry	0.5%	Depends on target preparation	Relatively small samples
Radiochemical separation followed by beta- and γ-ray counting	1-5%	Time consuming	Relatively large samples
Instrumental high-resolution γ-ray counting	1-5%	Fast, in-field analysis	Large samples
Na(I) measurements (From 1955 to 1965)	10%	Fast, in-field analysis	Large samples
Geiger-counter (Before 1955)	20%	Fast analysis	Large samples

Established destructive analysis methods, such as thermal ionization mass spectrometry and inductively coupled plasma mass spectrometry can effectively characterize uranium and plutonium isotopic content but require complete sample dissolution. This sample preparation requirement

challenges the timeliness goals provided by national and international agencies. Mass spectroscopic methods are often seen as the gold standard in isotopic analysis due to both high-fidelity identification and detection limits that can reach the femtogram range.

Unlike the current state-of-the-art (Table 1), our proposed approach takes full advantage of using high-resolution gamma-ray spectrometry to assay certain fission product yields. This has been the subject of several publications containing methods that have been developed to identify fissile materials and in some cases quantify their masses [13,14,16]. The work presented here provides a technique that will not necessarily surpass mass spectrometry in isotopic identification and quantification, but fills an important niche in fissile material characterization by providing rapid, high-fidelity of fissile identification without sample dissolution. As a result, fission from several actinides, such as ^{239}Pu, ^{235}U, and ^{238}U can be rapidly ascertained in field from unprocessed samples.

II. Characterization of Fission Species using Gamma-Ray Ratios

In prior progress reports we provided time-dependent fission-product gamma-ray ratios for 14 pairs obtained from the three major actinides after exposure of fissionable samples to monoenergetic neutron beams [1-5]. We reported the identification of gamma-ray line pairs that are prominent at different times in the gamma-ray spectra from the three fission samples (^{235}U, ^{238}U, and ^{239}Pu), and are sensitive to the target isotope or, separately, the incident neutron energy. In addition we are providing a new regression analysis of our experimental fission product yield (FPY) data relevant to Godiva FPY data and to the complementary (surrogate) photofission product yields of ^{240}Pu. The main advantage of the regression analysis is that it investigates the FPY data set as a whole, rather than focusing on individual FPY ratios. It is a statistical tool establishing the relationship between a dependent variable and one or more independent variables.

For the gamma-ray line ratios and for the regression analysis we used our experimentally measured fission product gamma-ray spectra from the "Big three" fissile targets: ^{235}U, ^{238}U and ^{239}Pu [1-5]. These experiments have been performed at the Triangle Universities Nuclear Laboratory (TUNL) using monoenergetic neutron beams (from 0.58 to 14.8 MeV) to induce (n,f) reactions under very well characterized conditions. The obtained data provides a rich source of pertinent experimental information that can be used to establish a baseline of gamma spectral information associated with specific fissioning isotopes at discrete energies.

III. Scientific basis for the gamma-ray ratio method

This study focuses on identifying gamma-ray line pairs and groups that are prominent at different times in the gamma-ray spectrum and that are sensitive to the fissile material or—separately—to the incident neutron energy. Fig. 1 shows the cumulative thermal fission product yields of ^{235}U and ^{239}Pu as a function of product mass. The main difference between the two curves is the significant shift to higher atomic mass number of the ^{239}Pu curve with respect to ^{235}U curve; the two distributions are sufficiently well defined so that the γ-ray emissions within the individual isobar pairs can be made to distinguish the fissioning species.

The observed fission product intensity ratios are independent of the number of fissions induced in the sample. By judicially choosing the pairs studied, the effects of γ-ray attenuation and detector

efficiency can be minimized. We can then form ratios from multiple peak pairs to enhance the confidence in the material identification. Table 2 lists a number of peak pairs useful in distinguishing between ^{239}Pu, ^{235}U, and ^{238}U.

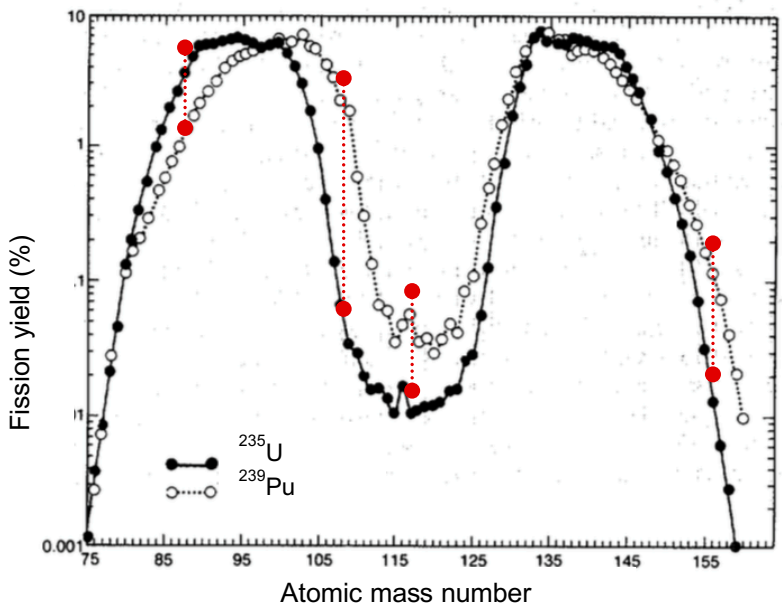

Fig. 1. Cumulative thermal fission product-yield distributions for ^{235}U and ^{239}Pu. Notice the prominent difference in the significant shift of the light mass peak toward the heavy mass peak as we transition form ^{235}U to ^{239}Pu. At the same time, the position of the heavy peak is largely independent of the mass of the fissionable nuclide. We can use these relationships to determine the species that underwent fission without requiring destructive assays.

Choosing the γ-rays used in forming intensity ratios requires consideration of a number of parameters including that the γ-rays must be relatively intense and unobscured by other peaks in the spectrum throughout the count period. The parent isotopes must have a half-life commensurate with the desired counting period, the induced fission rate, and the cooling period. The γ-rays should be sufficiently penetrating to readily escape from the sample. It is also beneficial if the peaks used in forming the intensity ratios be similar in energy so as to minimize the effects of matrix attenuation and variations in detector efficiency with energy

In Table 2 we identify some of the strongest gamma-ray lines associated with ^{238}U, ^{235}U, and ^{239}Pu fission products. The mass distribution of the fission products and the detailed time history of the measurements are some of the important factors that were considered. For example, the time history is important since there are variations in half-lives of the nuclides in the decay chains. We followed the decay time of each fission product in order to determine the best peak-to-background ratio. By following these criteria we were able to obtain the lowest detection limit and thus minimize the uncertainties in the determined FPY ratios. For this analysis we focused on the first few minutes to days of the fission gamma-ray spectra. These state-of-the-art fission product yield data contain rich γ-ray history with enormous information relevant for post detonation nuclear

forensics. Hence these gamma-ray ratios can be used to identify the material that underwent fission as are summarized in tables and graphs below.

Table 2. Nuclear spectroscopic data for identified fission products (from ENDF/B-VII.1).

Fragment	**E_γ (keV)**	**$T_{1/2}$**	**I_γ (%)**
91Sr	1024.3	9.63(5) h	33.50(1.10)
92Sr	1383.93	2.611(10) h	90(4)
95Zr	724.19	64.032(6) d	44.27(22)
97Zr	743.36	16.749(8) h	93.09(16)
99Mo	739.5	65.976(24) h	12.26(22)
103Ru	497.09	39.247(13) d	91.0(1.2)
105Ru	724.09	4.44(2) h	47.3(5)
127Sb	685.7	3.85(5) d	36.8(2.0)
131I	364.49	8.0252(6) d	81.5(8)
132Te	228.16	3.204(13) d	88(3)
133I	529.87	20.83(8) h	87.0(3)
135Xe	249.79	9.14(2) h	90(3)
136Cs	1048.07	13.16(3) d	80(3)
140Ba	537.26	12.7527(23) d	24.39(23)
143Ce	293.27	33.039(6) h	42.8(4)
147Nd	531.02	10.98(1) d	13.37(27)

Fig. 2 shows the optimal decay time for the fission product ^{92}Sr to minimize the peak uncertainty. This uncertainty was analyzed based on two constituent parts: the net photopeak area and the background distribution. The background distribution is very complex and changes over the decay time. The shaded region shows the optimal decay time to minimize the uncertainty of the net peak area for this particular fission product. We use this criteria for all peak pairs presented in Tables 3-16.

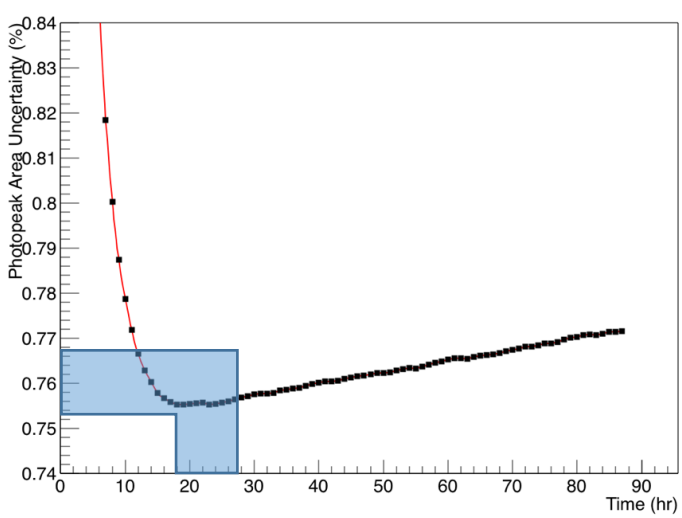

Fig. 2. The peak area uncertainty of the 1383.93 keV gamma-ray line emitted by ^{92}Sr as a function of decay time.

IV. Relevant Prior Work

In 2010, Lawrence Livermore National Laboratory (LLNL), Los Alamos National Laboratory (LANL), and the Triangle Universities Nuclear Laboratory (TUNL) formed a joint collaboration to measure the energy dependence of various high-yield fission products using monoenergetic neutrons in an accurate and self-consistent manner; the PI for this proposal, Anton Tonchev, is one of the senior members of the LLNL-LANL-TUNL collaboration and has direct access to the collaboration's data. The LLNL-LANL-TUNL team has measured the energy dependence of various high-yield fission products by using specially constructed dual-fission chambers and high-resolution γ-ray spectrometry. The dual-fission chambers each contained a thick (200–400 mg/cm^2) actinide target of ^{235,238}U or ^{239}Pu and two thin (~10–100 μg/cm^2) reference foils of the same actinide. We measured the cumulative yields of 16 fission products ranging from ^{92}Sr to ^{147}Nd and from 0.58 to 14.8 MeV [1-4]. This approach resulted in an accurate (1-2%) determination of the number of fissions that occurred in the thick target without requiring knowledge of the fission cross section or neutron fluence on target. Following neutron activation, we removed the thick target from the dual-fission chamber and continuously counted γ-rays for periods up to 3 months using large-volume HPGe detectors to determine the yield of various fission products. We have measured time-dependent fission-product gamma-ray spectra at eight incident neutron energies En = 0.58, 1.37, 2.37, 3.50, 4.49, 5.5, 8.9, and 14.8 MeV. The γ-ray counting started just 10 minutes after the end of irradiation and continued for a period of 3 months. To the extent possible, all irradiation and counting procedures were kept the same to minimize sources of systematic errors. These state-of-the-art fission product yield data contain rich γ-ray history with enormous information relevant for post detonation nuclear forensics.

V. Experimental Results

We identified gamma-ray line pairs that are prominent at different times in the gamma-ray spectrum and that are sensitive to the fissile material and to the incident neutron energy. By judicially choosing the pairs studied, the effects of γ-ray attenuation and detector efficiency was minimized. Ratios were then formed from multiple peak pairs to enhance the confidence in the material identification. Fission-product gamma-ray spectra were measured at eight monoenergetic incident neutron energies E_n = 0.58(0.03), 1.37(0.12), 2.37(0.07), 3.50(0.20), 4.49(0.25), 5.5(0.23), 8.9(0.25), and 14.8(0.15) MeV, where the values in parenthesis are the neutron energy spread (FWHM) in MeV. Tables 3-16 Lists, for eight incident neutron energies, the measured fission product gamma ray pairs that have been selected to distinguish between fission from ^{235}U, ^{238}U and ^{239}Pu.

Each table gives the incident neutron energy and the extracted photopeak ratios for the selected fission products for ^{235}U, ^{238}U and ^{239}Pu. The photopeak ratios have been corrected for the HPGe photopeak efficiency and the corresponding gamma-ray branching ratio, and thus also correspond to the FPY ratios. As shown in Tables 3-18 and corresponding Figures 3-18, the fission species can be unambiguously identified by forming ratios that come from different regions of the mass distribution. Some ^{238}U peak pairs from our TUNL measurements don't exhibit the smooth energy dependency seen in ^{235}U and ^{239}Pu. This is very obvious for our 9 MeV neutron data. The main reason is probably the relatively shorter irradiation (and counting) of ^{238}U compare to the other fission

species. In order to correct this deficiency our LLNL-LANL-TUNL collaboration recently remeasured the 9 MeV data for the three actinides.

For diagnostic purposes, we would like to have samples that have activities that are referred to as "refractory". Refractory elements are those that are present in the liquid droplets when they solidify. It has been found that these activities behave most like actinides in the environment, unlike "volatile" samples that are made up of elements that have high vapor pressures or have noble gasses (Kr or Xe) early in their decay chain. The later samples often have activities that have been significantly geometrically separated from the actinides and as such have less useful diagnostic value.

As mentioned above one can purposely choose the relative abundance of two gamma transitions that are close in energy but selected so that one gamma-ray line is representative of volatile products and the second is representative of refractory products. There are several useful pairs that can be measured in unprocessed fission products. One of these pairs which can be used for relative refractory-volatility determination are ^{147}Nd/^{140}Ba, ^{95}Zr/^{132}Te, ^{99}Mo/^{132}Te. They are shown in Figures, Tables 16, 17, 18, respectively. One can also estimate the efficiency of the device from the relative amounts of fission products and residual fuel in the debris without knowing the yield. In this case, if we measure the concentration of some fission product that chemically behaves like the fuel, ^{147}Nd for example, to get the number of fissions in the sample. Then one can measure the residual fuel concentration by mass spectrometry or alpha counting to get the total number of fuel atoms in the sample.

Our data [1-5] will also allow us to determine the ^{235}U enrichment by measuring the intensity ratios gamma-ray lines from certain pairs of fission products. For example, the FPY ratio of the same ^{92}Sr/^{105}Ru pair as a function of ^{235}U abundances (A) is given by the following relation [17]:

$$N(^{92}Sr)/N(^{105}Ru) = 1.2046\ EXP(0.7264*A)$$

By taking the 2.28 FPY ratio from Table XXIII from Ref. [1] at 14 MeV for ^{235}U, one can find out that ^{235}U enrichment was (88 +/- 6)%, which is in agreement with the experimental value of 94%.

Table 3. Intensity ratios of ^{91}Sr vs. ^{103}Ru fission product gamma rays as a function of the incident neutron energies.

En (MeV)	239Pu(n,f)		235U(n,f)			238U(n,f)
0.58	0.153	0.003	0.675	0.018	--	--
1.37	0.158	0.003	--	--	--	--
2.37	0.170	0.003	0.629	0.017	0.241	0.006
3.60	0.169	0.003	0.633	0.017	0.277	0.007
4.49	0.173	0.003	0.558	0.014	0.265	0.007
5.5	0.180	0.003	--	--	--	--
8.90	--	--	--	--	--	--
14.80	0.179	0.003	0.543	0.014	0.281	0.008

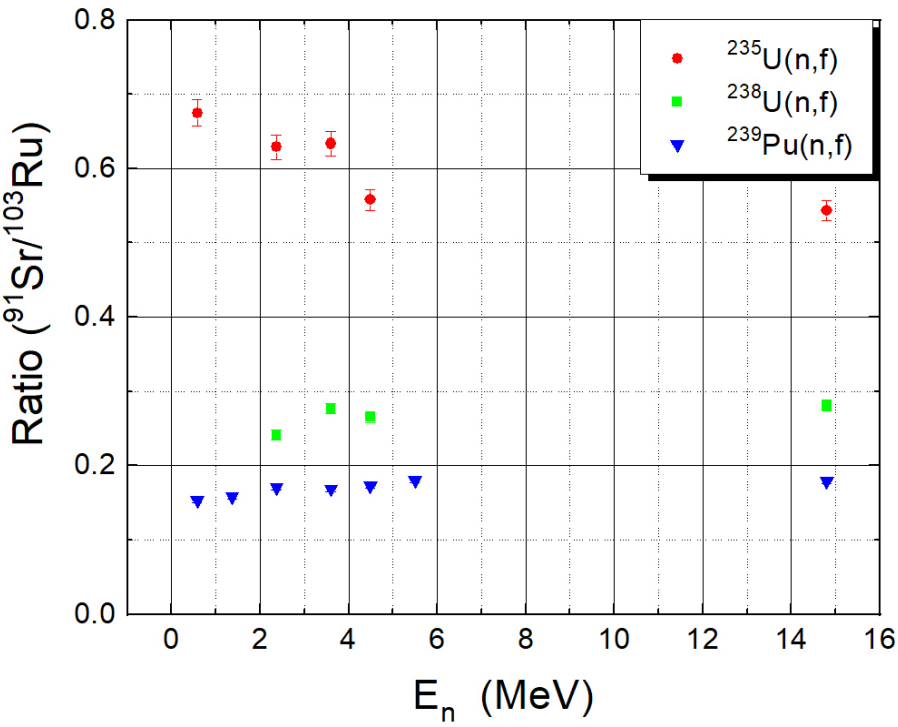

Fig. 3. Energy dependency of ^{91}Sr/^{103}Ru fission yield gamma-ray ratios from ^{235}U(n,f), ^{238}U(n,f) and ^{239}Pu(n,f).

Table 4. Intensity ratios of ^{91}Sr vs. ^{105}Ru fission product gamma rays as a function of the incident neutron energies.

En (MeV)	239Pu(n,f)		235U(n,f)		238U(n,f)	
0.58	0.340	0.006	3.895	0.110	--	--
1.37	0.365	0.007	3.681	0.077	0.777	0.028
2.37	0.410	0.008	2.523	0.050	0.639	0.017
3.60	0.406	0.008	2.355	0.043	0.643	0.017
4.49	0.412	0.011	2.459	0.051	0.629	0.025
5.5	--	--	--	--	--	--
8.90	--	--	--	--	--	--
14.80	0.439	0.018	1.601	0.033	0.791	0.029

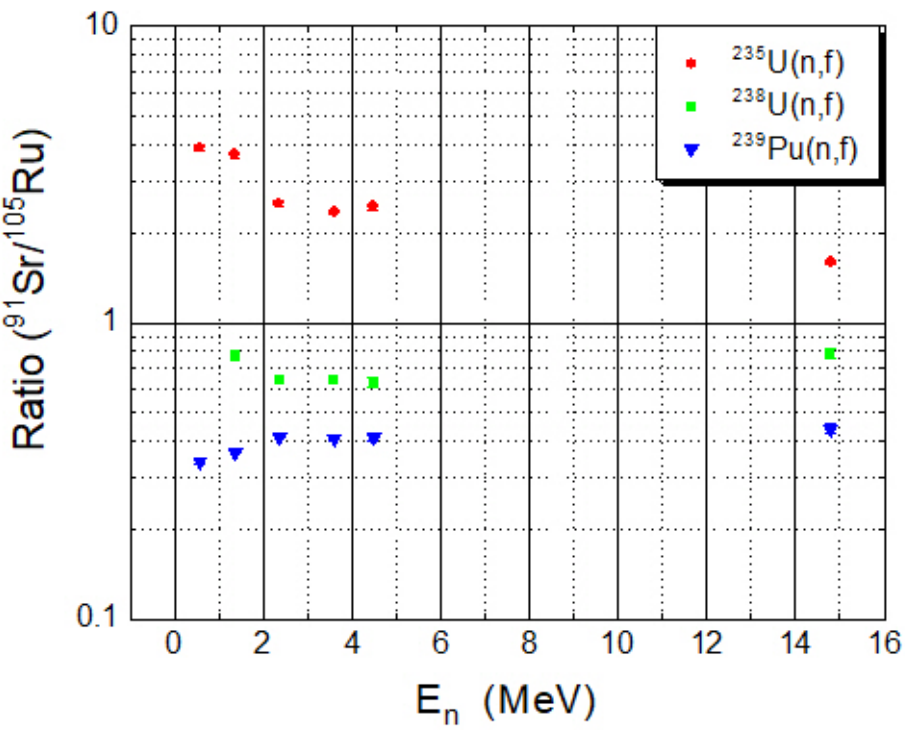

Fig. 4. Energy dependency of ^{91}Sr/^{105}Ru fission yield gamma-ray ratios from ^{235}U(n,f), ^{238}U(n,f) and ^{239}Pu(n,f).

Table 5. Intensity ratios of ^{91}Sr vs. ^{132}Te fission product gamma rays as a function of the incident neutron energies.

En (MeV)	239Pu(n,f)		235U(n,f)		238U(n,f)	
0.58	0.207	0.007	0.462	0.012	--	--
1.37	0.203	0.006	0.423	0.012	0.345	0.012
2.37	0.222	0.007	0.428	0.011	0.294	0.008
3.60	0.222	0.006	0.426	0.011	0.327	--
4.49	0.224	0.006	0.388	0.010	0.313	0.01
5.5	0.242	0.007	--	--	--	--
8.90	--	--	--	--	--	--
14.80	0.314	0.011	0.425	0.011	0.279	0.008

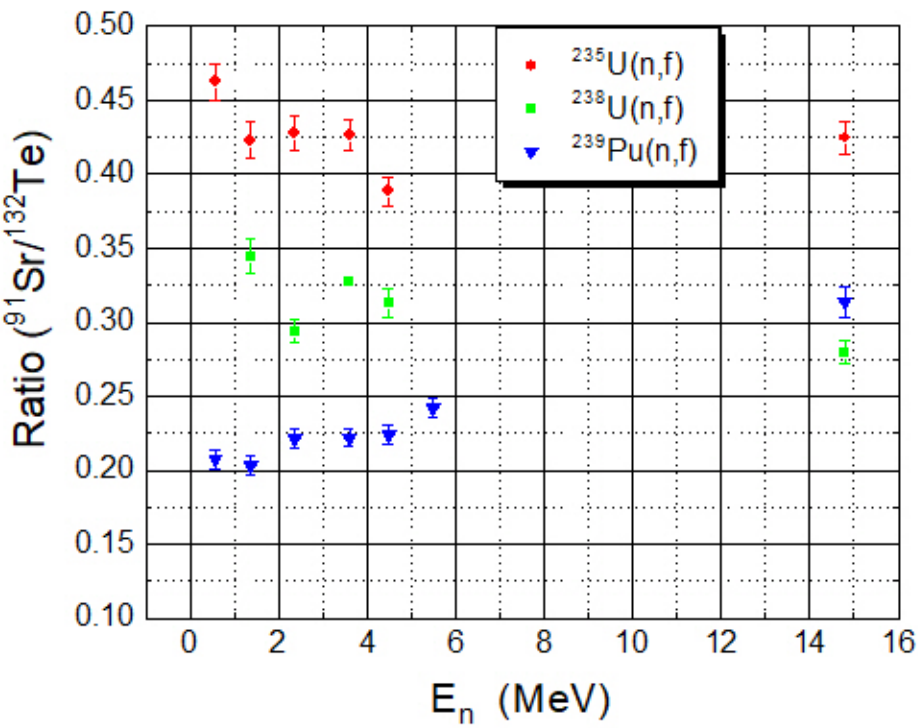

Fig. 5. Energy dependency of ^{91}Sr/^{132}Te fission yield gamma-ray ratios from ^{235}U(n,f), ^{238}U(n,f) and ^{239}Pu(n,f).

Table 6. Intensity ratios of ^{91}Sr vs. ^{133}I fission product gamma rays as a function of the incident neutron energies.

En (MeV)	239Pu(n,f)		235U(n,f)		238U(n,f)	
0.58	0.156	0.001	0.322	0.009	--	--
1.37	0.161	0.000	0.309	0.009	0.232	0.007
2.37	0.171	0.000	0.323	0.009	0.231	0.006
3.60	0.170	0.000	0.322	0.008	0.24	0.006
4.49	0.180	0.000	0.307	0.008	0.237	0.006
5.5	0.182	0.000	--	--	--	--
8.90	--	--	--	--	--	--
14.80	0.215	0.001	0.340	0.009	0.24	0.006

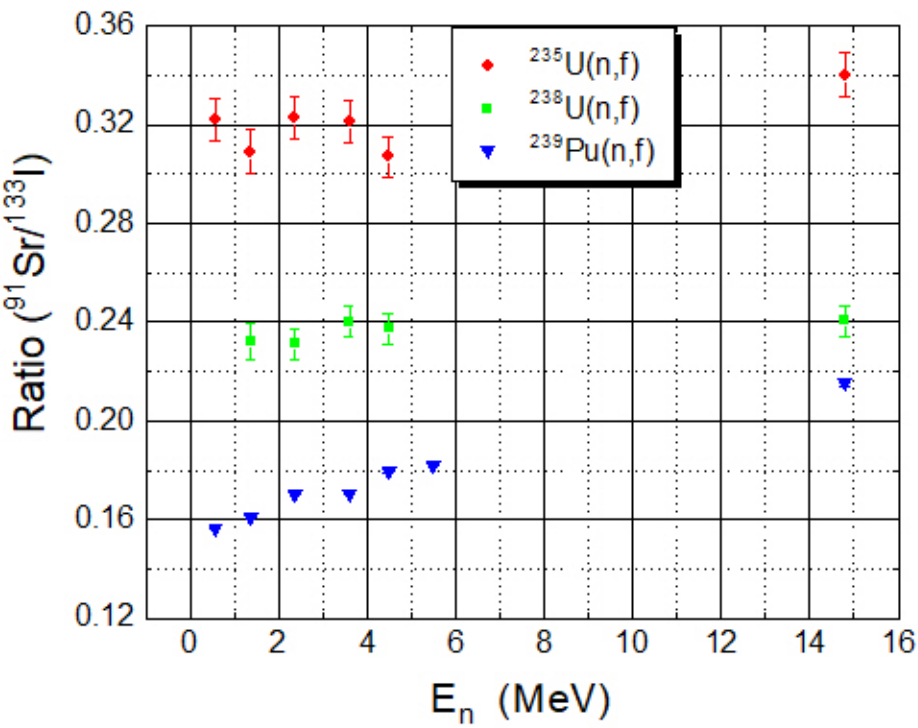

Fig. 6. Energy dependency of ^{91}Sr/^{133}I fission yield gamma-ray ratios from ^{235}U(n,f), ^{238}U(n,f) and ^{239}Pu(n,f).

Table 7. Intensity ratios of ^{91}Sr vs. ^{140}Ba fission product gamma rays as a function of the incident neutron energies.

En (MeV)	239Pu(n,f)		235U(n,f)		238U(n,f)	
0.58	0.696	0.024	1.385	0.037	--	--
1.37	0.738	0.021	1.18	0.033	1.014	0.037
2.37	0.794	0.022	1.327	0.034	0.945	0.028
3.60	0.786	0.022	1.389	0.036	1.014	--
4.49	0.809	0.027	1.298	0.034	0.981	0.033
5.5	0.845	0.023	--	--	--	--
8.90	--	--	--	--	--	--
14.80	0.911	0.035	1.419	0.038	1.066	0.038

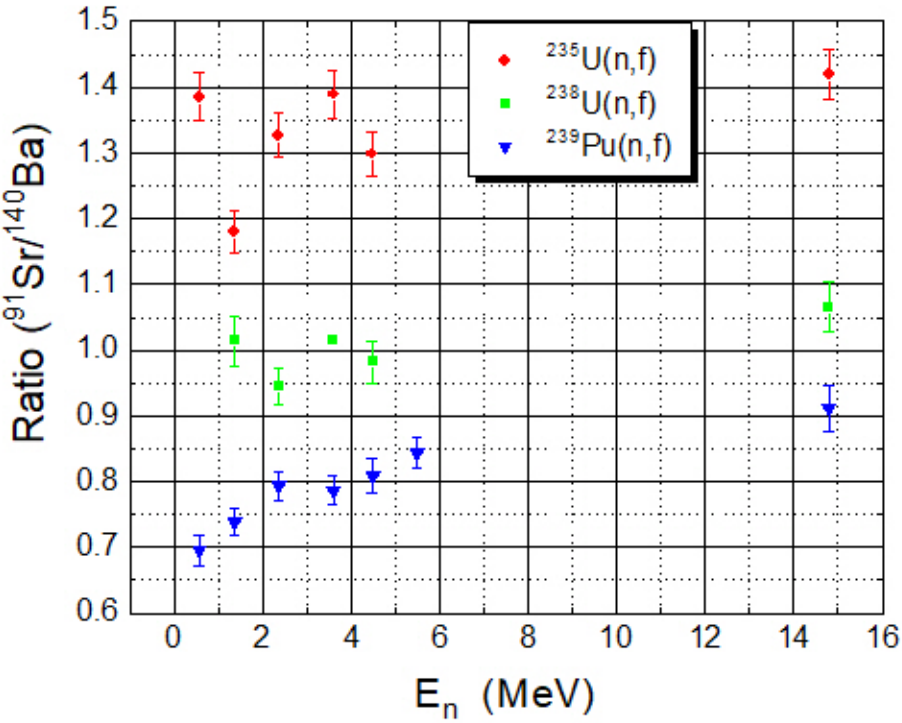

Fig. 7. Energy dependency of ^{91}Sr/^{140}Ba fission yield gamma-ray ratios from ^{235}U(n,f), ^{238}U(n,f) and ^{239}Pu(n,f).

Table 8. Intensity ratios of ^{91}Sr vs. ^{143}Ce fission product gamma rays as a function of the incident neutron energies.

En (MeV)	239Pu(n,f)		235U(n,f)		238U(n,f)	
0.58	0.497	0.014	0.781	0.021	--	--
1.37	0.507	0.015	0.711	0.022	0.733	0.03
2.37	0.557	0.016	0.786	0.021	0.67	0.018
3.60	0.540	0.015	0.837	0.021	0.748	0.02
4.49	0.555	0.022	0.831	0.023	0.686	0.019
5.5	0.601	0.018	--	--	--	--
8.90	--	--	--	--	--	--
14.80	0.707	0.025	0.926	0.025	0.709	0.02

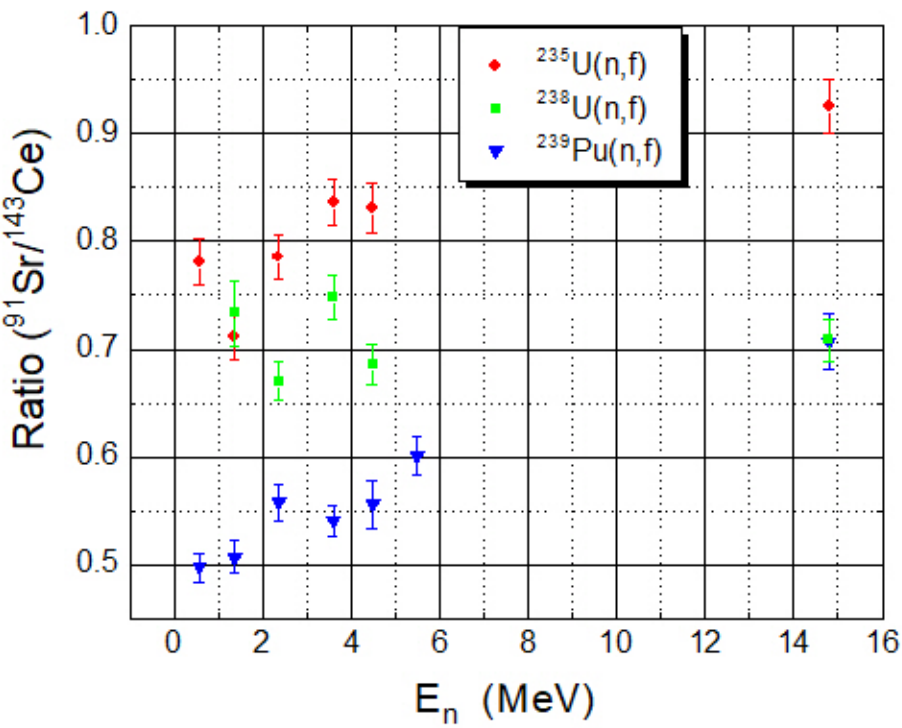

Fig. 8. Energy dependency of ^{91}Sr/^{143}Ce fission yield gamma-ray ratios from ^{235}U(n,f), ^{238}U(n,f) and ^{239}Pu(n,f).

Table 9. Intensity ratios of ^{91}Sr vs. ^{147}Nd fission product gamma rays as a function of the incident neutron energies.

En (MeV)	239Pu(n,f)		235U(n,f)		238U(n,f)	
0.58	3.415	0.100	6.763	0.227	--	--
1.37	3.352	0.084	5.762	0.157	4.045	0.196
2.37	3.490	0.101	6.127	0.180	3.745	0.118
3.60	3.473	0.090	6.929	0.191	--	--
4.49	3.326	0.108	6.082	0.184	3.791	0.133
5.5	--	--	--	--	--	--
8.90	--	--	--	--	--	--
14.80	3.884	0.145	7.398	0.203	4.302	0.147

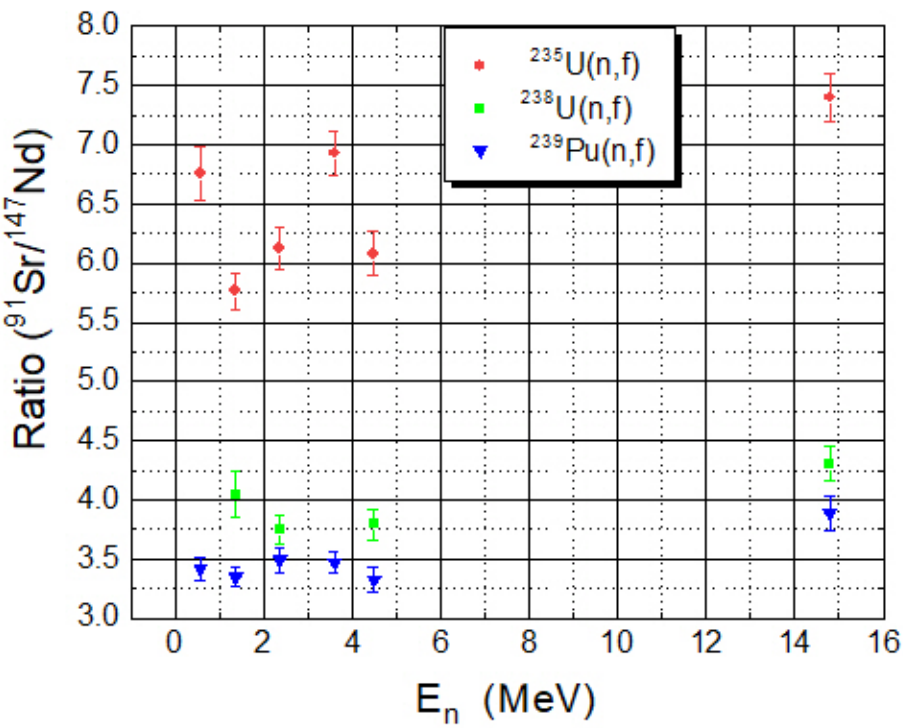

Fig. 9. Energy dependency of ^{91}Sr/^{147}Nd fission yield gamma-ray ratios from ^{235}U(n,f), ^{238}U(n,f) and ^{239}Pu(n,f).

Table 10. Intensity ratios of ^{92}Sr vs. ^{103}Ru fission product gamma rays as a function of the incident neutron energies.

En (MeV)	239Pu(n,f)		235U(n,f)		238U(n,f)	
0.58	0.468	0.013	1.854	0.053	--	--
1.37	0.472	0.012	--	--	--	--
2.37	0.489	0.014	1.683	0.045	0.684	0.018
3.60	0.473	0.013	1.802	0.049	0.847	0.023
4.49	0.491	0.014	1.531	0.041	0.713	0.021
5.5	0.494	0.013	--	--	--	--
8.90	--	--	--	--	--	--
14.80	0.489	0.014	1.470	0.039	0.8	0.021

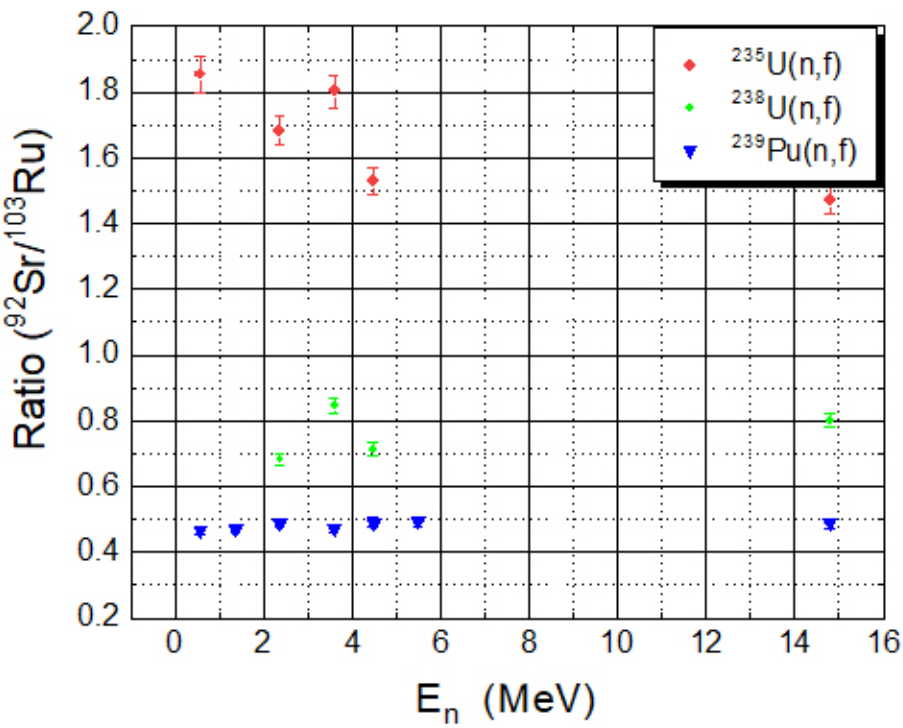

Fig. 10. Energy dependency of ^{92}Sr/^{103}Ru fission yield gamma-ray ratios from ^{235}U(n,f), ^{238}U(n,f) and ^{239}Pu(n,f).

Table 11. Intensity ratios of ^{92}Sr vs. ^{105}Ru fission product gamma rays as a function of the incident neutron energies.

En (MeV)	239Pu(n,f)		235U(n,f)		238U(n,f)	
0.58	1.038	0.028	10.698	0.382	--	--
1.37	1.089	0.029	10.287	0.335	2.397	0.088
2.37	1.178	0.034	6.754	0.184	1.812	0.048
3.60	1.140	0.033	6.700	0.178	1.967	0.055
4.49	1.169	0.040	6.752	0.193	1.690	0.071
5.5	--	--	--	--	--	--
8.90	1.087	0.047	--	--	1.973	0.061
14.80	1.197	0.055	4.331	0.127	2.230	0.080

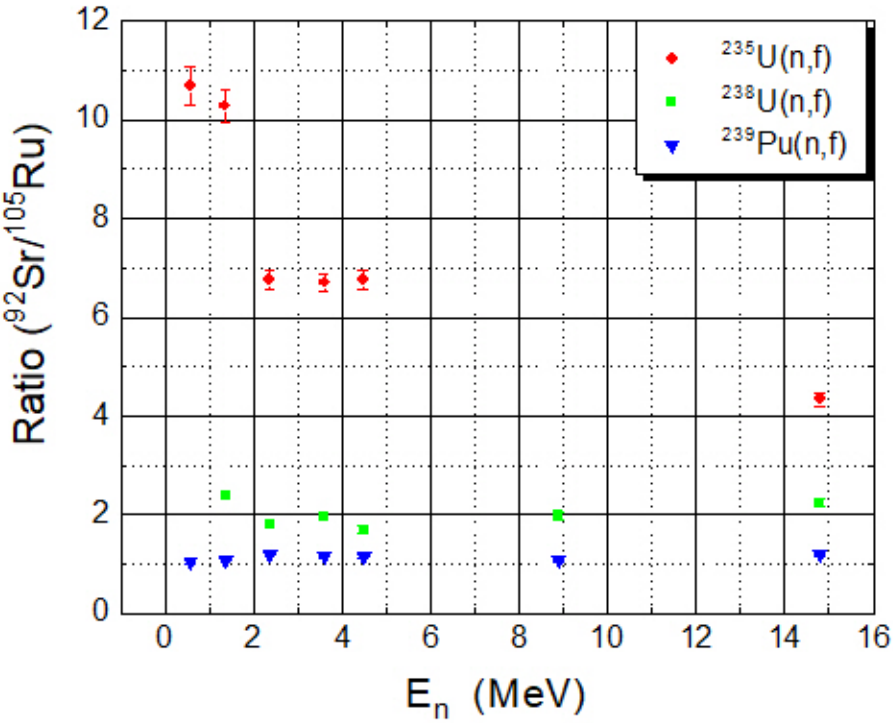

Fig. 11. Energy dependency of ^{92}Sr/^{105}Ru fission yield gamma-ray ratios from ^{235}U(n,f), ^{238}U(n,f) and ^{239}Pu(n,f).

Table 12. Intensity ratios of ^{92}Sr vs. ^{132}Te fission product gamma rays as a function of the incident neutron energies.

En (MeV)	239Pu(n,f)		235U(n,f)		238U(n,f)	
0.58	0.632	0.020	1.270	0.037	--	--
1.37	0.607	0.018	1.182	0.038	1.064	0.037
2.37	0.636	0.021	1.144	0.030	0.833	0.023
3.60	0.623	0.018	1.213	0.031	1	--
4.49	0.636	0.019	1.067	0.029	0.84	0.029
5.5	0.664	0.018	--	--	--	--
8.90	0.726	0.037	1.241	0.149	0.787	0.032
14.80	0.855	0.029	1.149	0.031	0.788	0.021

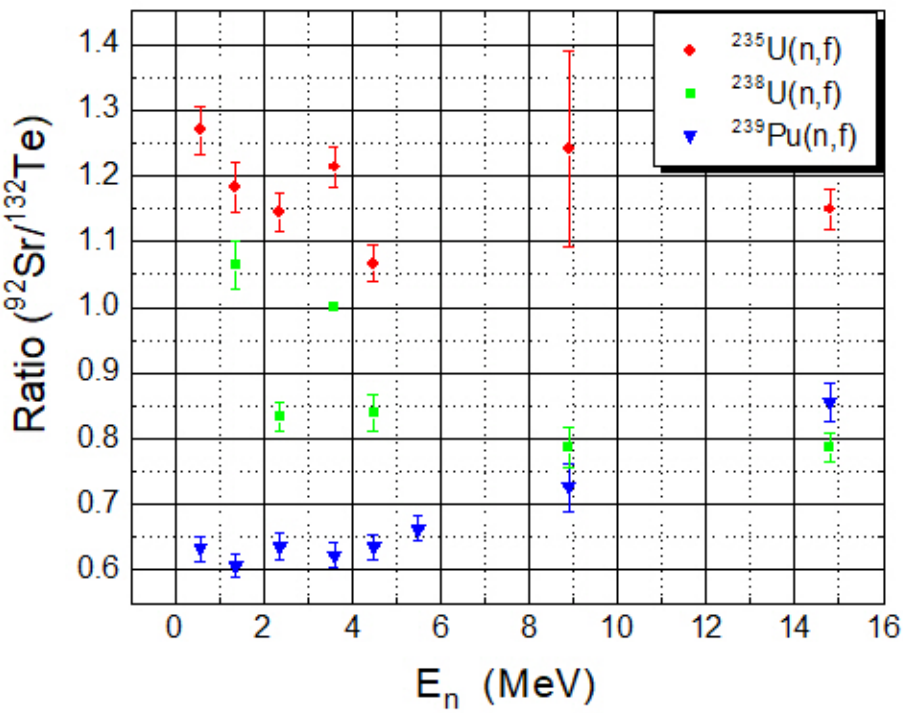

Fig. 12. Energy dependency of ^{92}Sr/^{132}Te fission yield gamma-ray ratios from ^{235}U(n,f), ^{238}U(n,f) and ^{239}Pu(n,f).

Table 13. Intensity ratios of ^{92}Sr vs. ^{140}Ba fission product gamma rays as a function of the incident neutron energies.

En (MeV)	239Pu(n,f)		235U(n,f)		238U(n,f)	
0.58	2.124	0.071	3.805	0.110	--	--
1.37	2.202	0.058	3.296	0.103	3.128	0.115
2.37	2.280	0.065	3.551	0.092	2.679	0.079
3.60	2.206	0.064	3.952	0.106	3.102	--
4.49	2.293	0.079	3.564	0.097	2.637	0.097
5.5	2.314	0.063	--	--	--	--
8.90	2.280	0.107	3.259	0.141	--	--
14.80	2.485	0.094	3.839	0.108	3.006	0.105

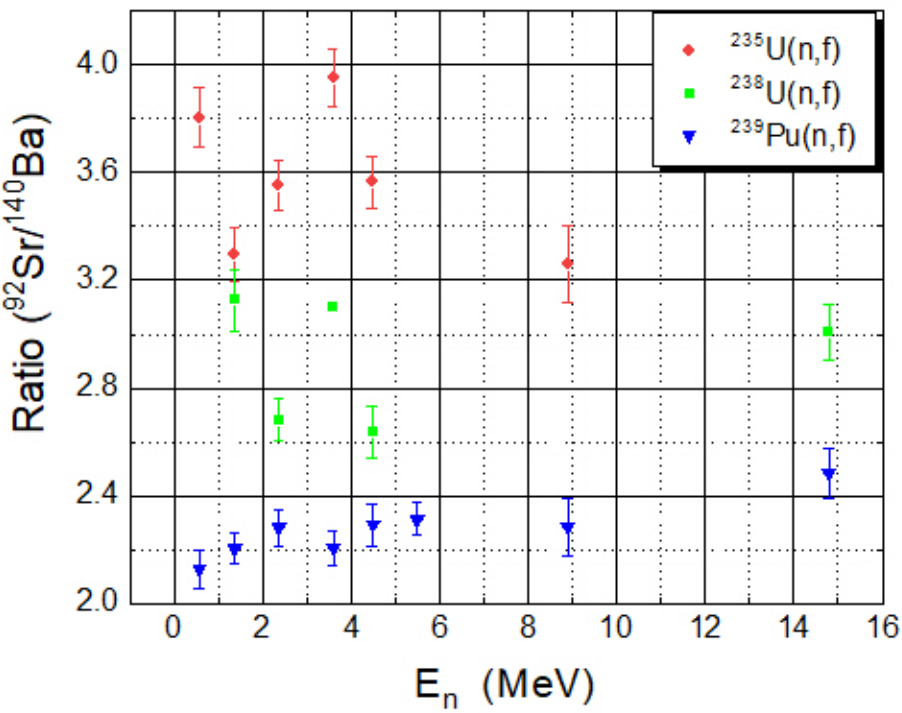

Fig. 13. Energy dependency of ^{92}Sr/^{140}Ba fission yield gamma-ray ratios from ^{235}U(n,f), ^{238}U(n,f) and ^{239}Pu(n,f).

Table 14. Intensity ratios of ^{92}Sr vs. ^{143}Ce fission product gamma rays as a function of the incident neutron energies.

En (MeV)	239Pu(n,f)		235U(n,f)		238U(n,f)	
0.58	1.517	0.040	2.146	0.062	--	--
1.37	1.513	0.044	1.988	0.069	2.415	0.088
2.37	1.601	0.049	2.103	0.055	2.219	0.059
3.60	1.515	0.044	2.381	0.062	2.396	0.066
4.49	1.575	0.064	2.281	0.066	2.103	0.065
5.5	1.647	0.048	--	--	--	--
8.90	1.647	0.072	2.147	0.178	--	--
14.80	1.929	0.069	2.504	0.070	2.207	0.059

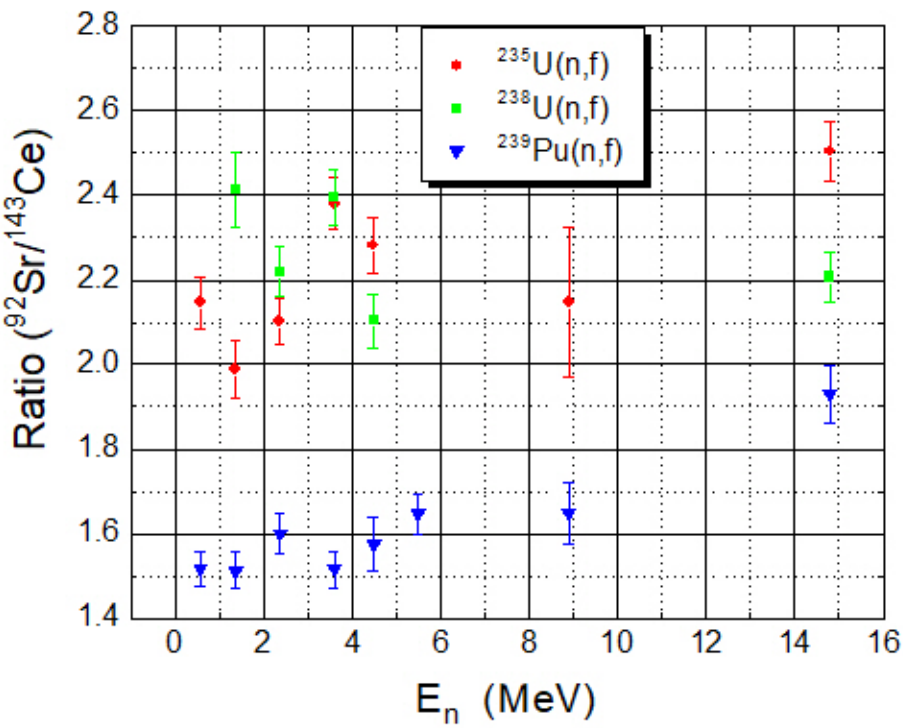

Fig. 14. Energy dependency of ^{92}Sr/^{143}Ce fission yield gamma-ray ratios from ^{235}U(n,f), ^{238}U(n,f) and ^{239}Pu(n,f).

Table 15. Intensity ratios of ^{92}Sr vs. ^{147}Nd fission product gamma rays as a function of the incident neutron energies.

En (MeV)	239Pu(n,f)		235U(n,f)		238U(n,f)	
0.58	10.607	0.292	18.616	0.657	--	--
1.37	10.167	0.238	16.136	0.502	12.508	0.611
2.37	10.046	0.301	16.437	0.483	10.64	0.33
3.60	9.315	0.252	19.758	0.553	--	--
4.49	9.370	0.314	16.736	0.522	10.206	0.388
5.5	9.208	--	--	--	--	--
8.90	9.935	0.579	16.326	0.317	10.263	0.555
14.80	10.746	0.403	20.056	0.582	12.157	0.41

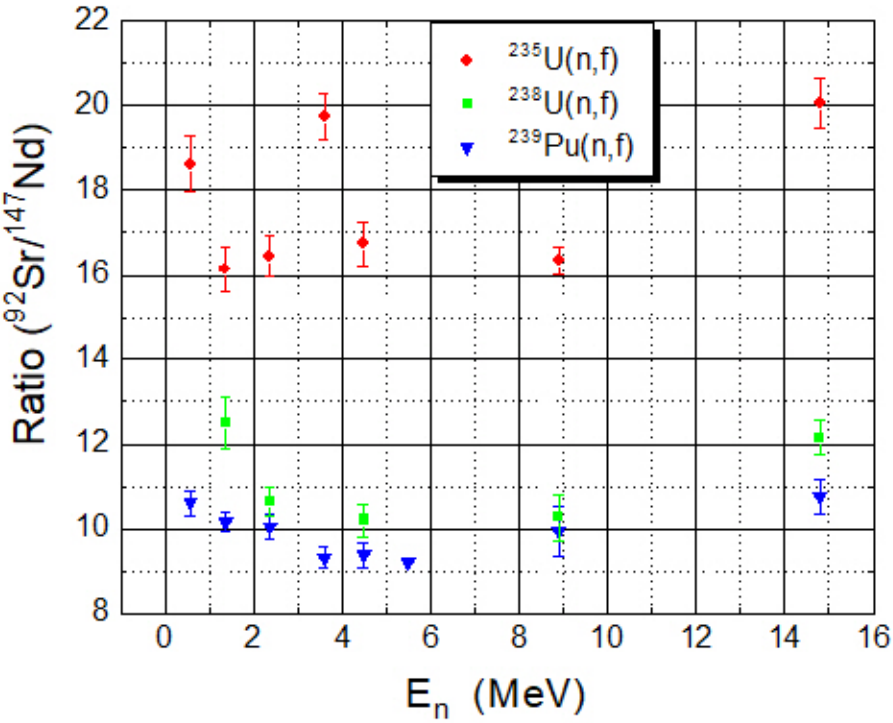

Fig. 15. Energy dependency of ^{92}Sr/^{147}Nd fission yield gamma-ray ratios from ^{235}U(n,f), ^{238}U(n,f) and ^{239}Pu(n,f).

Table 16. Intensity ratios of ^{147}Nd vs. ^{140}Ba fission product gamma rays as a function of the incident neutron energies.

En (MeV)	239Pu(n,f)		235U(n,f)		238U(n,f)	
0.58	0.200	0.007	0.204	0.007	--	--
1.37	0.217	0.005	0.204	0.005	0.25	0.012
2.37	0.227	0.007	0.216	0.006	0.252	0.009
3.60	0.237	0.006	0.200	0.006	--	--
4.49	0.245	0.009	0.213	0.007	0.258	0.01
5.5	0.251	--	--	--	--	--
8.90	0.230	0.014	0.200	0.008	--	--
14.80	0.231	0.010	0.191	0.005	0.247	0.01

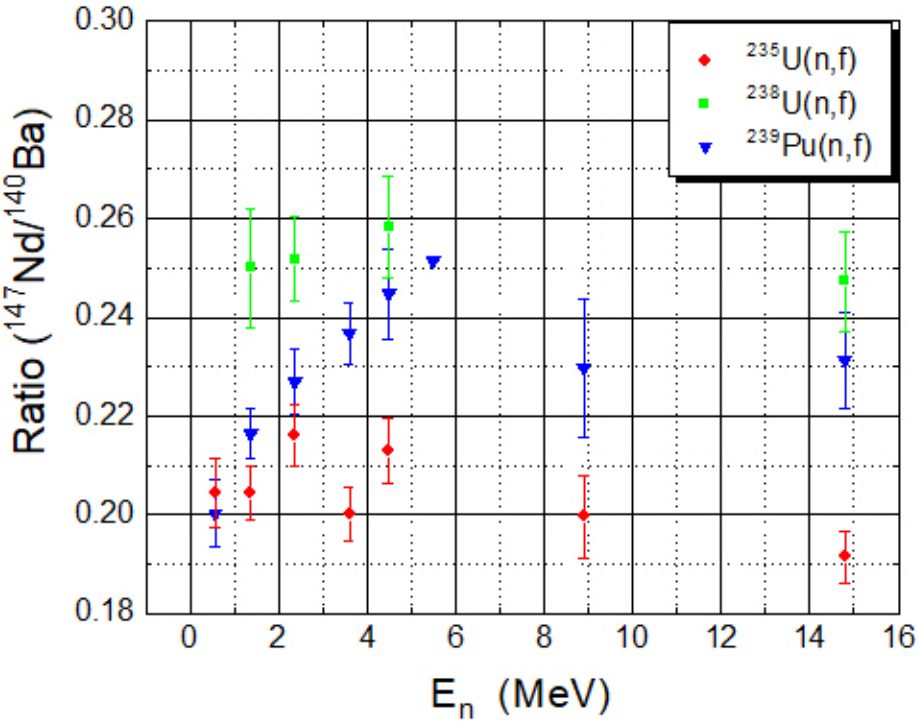

Fig. 16. Energy dependency of ^{147}Nd /^{140}Ba fission yield gamma-ray ratios from ^{235}U(n,f), ^{238}U(n,f) and ^{239}Pu(n,f).

Table 17. Intensity ratios of ^{95}Zr vs. ^{132}Te fission product gamma rays as a function of the incident neutron energies.

En (MeV)	239Pu(n,f)		235U(n,f)		238U(n,f)	
0.58	0.479	0.015	0.652	0.020	--	--
1.37	0.470	0.014	--	--	--	--
2.37	0.497	0.016	0.641	0.017	0.478	0.013
3.60	0.504	0.014	0.626	0.015	0.515	--
4.49	0.501	0.014	--	--	0.526	0.016
5.5	0.539	0.015	--	--	--	--
8.90	--	--	--	--	--	--
14.80	0.683	0.021	0.640	0.016	0.494	0.014

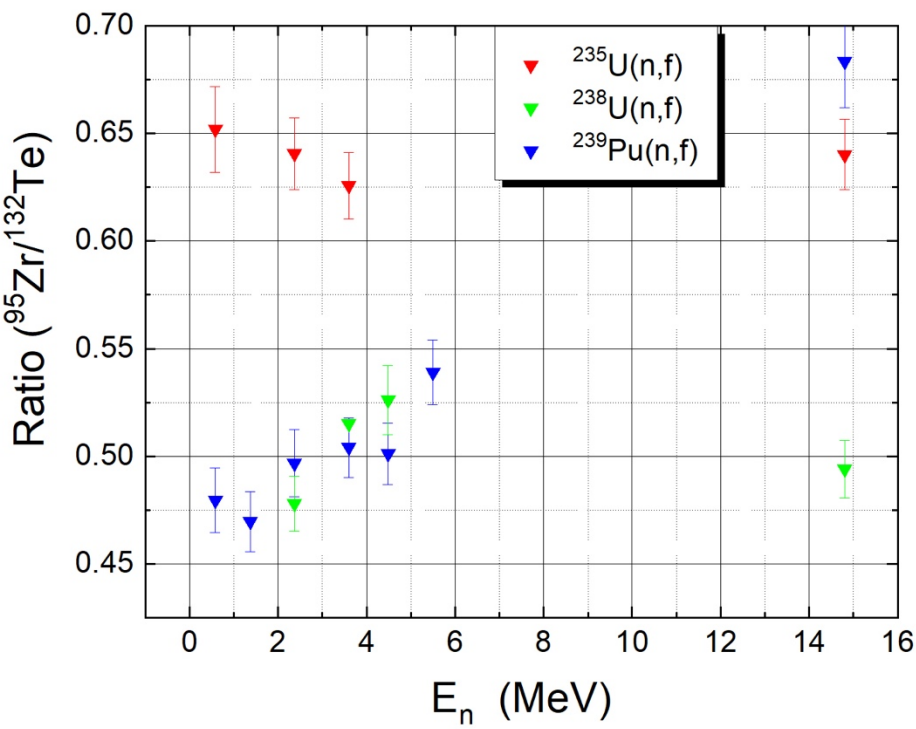

Fig. 17. Energy dependency of ^{95}Zr/^{132}Te fission yield gamma-ray ratios from ^{235}U(n,f), ^{238}U(n,f) and ^{239}Pu(n,f).

Table 18. Intensity ratios of ^{99}Mo vs. ^{132}Te fission product gamma rays as a function of the incident neutron energies.

En (MeV)	239Pu(n,f)		235U(n,f)		238U(n,f)	
0.58	0.185	0.006	0.172	0.005	--	--
1.37	0.179	0.005	0.179	0.005	0.176	0.005
2.37	0.181	0.006	0.168	0.004	0.167	0.005
3.60	0.177	0.005	0.174	0.004	0.179	--
4.49	0.179	0.005	0.160	0.004	0.182	0.006
5.5	0.189	0.006	--	--	--	--
8.90	0.197	0.009	0.181	0.022	0.168	0.006
14.80	0.237	0.008	0.165	0.005	0.159	0.004

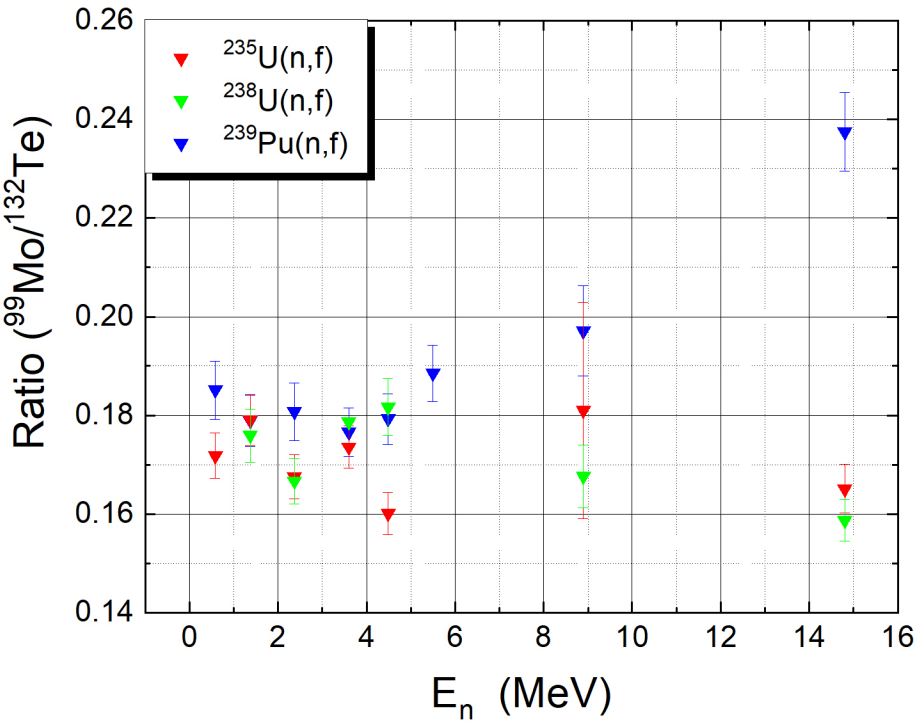

Fig. 18. Energy dependency of ^{99}Mo/^{132}Te fission yield gamma-ray ratios from ^{235}U(n,f), ^{238}U(n,f) and ^{239}Pu(n,f).

VI. Characterization of Fission Species using Multiple Fission Isotopes

In addition to the fission product-yield ratios we have used a regression analysis with our extensively measured fission product yield data to extract information relevant to the nuclear forensic effort. The main advantage of this analysis is that instead of following up on individual FPY ratios we are able to investigate the FPY data set as a whole. This is a statistical tool that allows us to extract unknown values of one variable based on known values of other variables. Of course the correlation analysis can only uncovers a relationship; it cannot provide a conclusive reason for why there's a relationship or reveal which variable influences the other.

Table 19 presents a summary of the relevant measured cumulative fission yields for two different neutron energies: 1) 2.37 MeV that is characteristic of the fission neutron spectrum and 2) 14.8 MeV that provides information on the thermonuclear induced fission region. The listed isotopes have readily identifiable characteristic gamma rays and half-lives that are amenable to in field nuclear forensic analysis.

Table 19. Cumulative measured fission product yields.

Isotope	T 1/2 (hr)	235U %/f (2.37)	238U %/f (2.37)	239Pu %/f (2.37)	235U %/f (14.8)	238U%/f (14.8)	239Pu%/f (14.8)
91Sr	9.6	5.38	4.17	3.19	4.34	3.65	2.62
92Sr	2.6	5.36	4.40	3.41	4.37	3.82	2.66
95Zr	1536	6.10	5.13	5.41	4.95	4.87	4.32
97Zr	16.7	5.94	5.62	5.93	4.88	4.97	4.74
99Mo	66	5.76	6.46	7.11	4.61	5.66	5.42
103Ru	939.36	3.15	6.36	6.90	2.94	4.72	5.38
105Ru	4.44	1.51	4.62	5.51	1.92	3.26	4.23
127Sb	92.4	0.33		0.73	1.64		2.27
131I	192.48	3.23	3.18		4.43	3.94	
132Te	76.8	4.79	5.40	5.48	3.89	4.96	3.18
133I	20.8	6.42	6.94	7.20	4.91	5.83	4.69
135Xe	9.14	6.48	7.77	8.44	5.36	5.74	5.27
136Cs	316.8			0.16			0.82
140Ba	306	5.57	6.06	5.52	4.20	4.69	3.95
143Ce	33.04	5.36	4.87	4.48	3.67	4.02	2.90
147Nd	263.52	2.20	2.68	2.29	1.47	2.10	1.67

Figure 19 presents the ratio of these data to the England-Rider predictions. The majority of the measurements are consistent with the predictions. Some of the lower yield species (eg ^{127}Sb and ^{136}Cs) show larger variations.

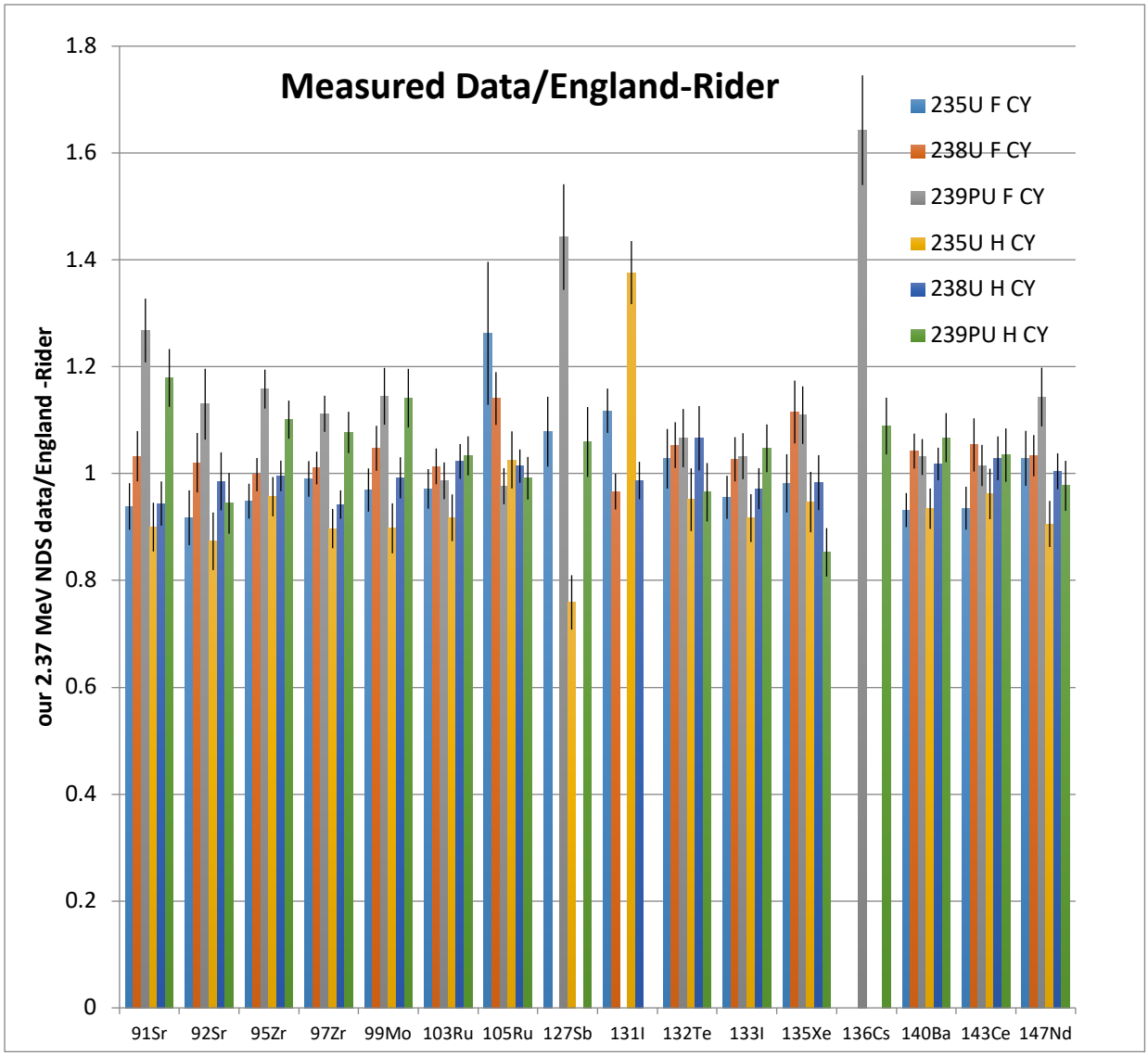

Figure 19. Ratio of the measured cumulative yields to the predictions of England-Rider. The errors shown in the figure are the experimental reported values [1].

It should be stressed that for forensic applications the number of fissions will be unknown as will be the cumulative yield for specific fission products. The distinct advantage offered by a direct spectral comparison of various fission product gamma rays is that many of the sources of error associated with determining the absolute fission product yield such as the total number of fissions, the "bomb fraction" present in the sample and the nuclear spectroscopic gamma-ray branching ratios are not required. The only parameters needed for this analysis are the half-lives of the isotopes (these are well known) and some knowledge of the relative (not absolute) gamma ray detection efficiency.

To demonstrate the power of this procedure the data in Table 20 were utilized as input to a regression analysis where "observed" data (i.e. the type of data that would be obtained in field at a detonation site) were randomized to simulate experimental uncertainties and can include contributions from various fissile species.

First a simple example. Table 20 shows a case where all the fissions comes from ^{239}Pu for neutrons from the fission neutron spectrum.

Table 20. Regression analysis to determine contribution of fission species to "observed" values. In this example the input assumption is that all fissions were induced on ^{239}Pu by fission spectrum neutrons and there were no experimental errors in the observation.

Isotope	235U F CY	238U F CY	239PU F CY	235U H CY	238U H CY	239PU H CY	"Observed"
91Sr	5.38	4.17	3.19	4.34	3.65	2.62	3.19
92Sr	5.36	4.40	3.41	4.37	3.82	2.66	3.41
95Zr	6.10	5.13	5.41	4.95	4.87	4.32	5.41
97Zr	5.94	5.62	5.93	4.88	4.97	4.74	5.93
99Mo	5.76	6.46	7.11	4.61	5.66	5.42	7.11
103Ru	3.15	6.36	6.90	2.94	4.72	5.38	6.90
105Ru	1.51	4.62	5.51	1.92	3.26	4.23	5.51
132Te	4.79	5.40	5.48	3.89	4.96	3.18	5.48
133I	6.42	6.94	7.20	4.91	5.83	4.69	7.20
135Xe	6.48	7.77	8.44	5.36	5.74	5.27	8.44
140Ba	5.57	6.06	5.52	4.20	4.69	3.95	5.52
143Ce	5.36	4.87	4.48	3.67	4.02	2.90	4.48
147Nd	2.20	2.68	2.29	1.47	2.10	1.67	2.29
Input	0	0	1	0	0	0	
Calculated	0	0	1	0	0	0	
Error	0	0	0	0	0	0	

The regression analysis correctly shows that all fission comes from fission spectrum neutrons on ^{239}Pu and there is no "error" in the analysis.

As a second, more realistic example (Table 21), the assumption remains that all fissions are from fission spectrum neutrons on ^{239}Pu but in this case the "observed" values are randomized by an assumed 3% uncertainty in the measured data. In this case the regression analysis still clearly shows the fissioning species is fission spectrum induced ^{239}Pu (97.2 (4.1)%) but there are now uncertainties introduced from the randomized "observed" input data. The other fission candidates are consistent with null contribution to the "observed" fission value.

A more complex example is presented in Table 22. In this case it is assumed: 50% of the fissions are from fission spectrum neutrons on ^{239}Pu; 30% of the fissions come from 14.8 MeV induced fission of ^{238}U; and 20% of fissions from fission spectrum neutrons on ^{235}U. In all cases the input data was randomized to have a 3% uncertainly due to the assumed experimental statistical errors.

Even for this complex case the regression analysis gives a very good determination of the contributions of the fissioning species and would be extremely valuable in characterizing the device composition and sophistication. With these successes, this procedure should be further vetted using existing experimental data obtained in the US Nuclear Testing Program.

Table 21. Same assumptions as Table 20 but in this case the "observed" values were randomized with an assumed 3% uncertainty in the experimental data.

Isotope	235U F CY	238U F CY	239PU F CY	235U H CY	238U H CY	239PU H CY	"Observed"
91Sr	5.38	4.17	3.19	4.34	3.65	2.62	3.22
92Sr	5.36	4.40	3.41	4.37	3.82	2.66	3.36
95Zr	6.10	5.13	5.41	4.95	4.87	4.32	5.42
97Zr	5.94	5.62	5.93	4.88	4.97	4.74	5.98
99Mo	5.76	6.46	7.11	4.61	5.66	5.42	7.05
103Ru	3.15	6.36	6.90	2.94	4.72	5.38	6.87
105Ru	1.51	4.62	5.51	1.92	3.26	4.23	5.57
132Te	4.79	5.40	5.48	3.89	4.96	3.18	5.50
133I	6.42	6.94	7.20	4.91	5.83	4.69	7.12
135Xe	6.48	7.77	8.44	5.36	5.74	5.27	8.40
140Ba	5.57	6.06	5.52	4.20	4.69	3.95	5.57
143Ce	5.36	4.87	4.48	3.67	4.02	2.90	4.44
147Nd	2.20	2.68	2.29	1.47	2.10	1.67	2.29
Input	0	0	1.0	0	0	0	
Calculated	-0.048	0.012	0.972	0.062	0.062	0.016	
Error	0.051	0.046	0.041	0.066	0.066	0.039	

Table 22. Similar to Tables 20 and 21 but with the assumption that the fissions come: 50% from fission spectrum induced fission of ^{239}Pu, 30% from 14.8 MeV induced fission of ^{238}U, and 20% from fission spectrum induced fission of ^{235}U.

Isotope	235U F CY	238U F CY	239PU F CY	235U H CY	238U H CY	239PU H CY	"Observed"
91Sr	5.38	4.17	3.19	4.34	3.65	2.62	3.80
92Sr	5.36	4.40	3.41	4.37	3.82	2.66	3.93
95Zr	6.10	5.13	5.41	4.95	4.87	4.32	5.37
97Zr	5.94	5.62	5.93	4.88	4.97	4.74	5.61
99Mo	5.76	6.46	7.11	4.61	5.66	5.42	6.40
103Ru	3.15	6.36	6.90	2.94	4.72	5.38	5.52
105Ru	1.51	4.62	5.51	1.92	3.26	4.23	4.06
132Te	4.79	5.40	5.48	3.89	4.96	3.18	5.20
133I	6.42	6.94	7.20	4.91	5.83	4.69	6.67
135Xe	6.48	7.77	8.44	5.36	5.74	5.27	7.29
140Ba	5.57	6.06	5.52	4.20	4.69	3.95	5.24
143Ce	5.36	4.87	4.48	3.67	4.02	2.90	4.49
147Nd	2.20	2.68	2.29	1.47	2.10	1.67	2.21
Input	0.2	0	0.5	0	0.3	0	
Calculated	0.150	0.017	0.516	0.063	0.290	-0.034	
Error	0.026	0.024	0.021	0.034	0.030	0.020	

A. Constrained Regression Analysis of Fission Product Yields

Using fission product yield data from the extensive measurements we have obtained at TUNL we have performed constrained regression analyses on 4 different data sets obtained from Godiva critical assembly measurements [6]. As a proxy for nuclear forensics analysis on uncharacterized nuclear explosions we have attempted to determine if it would be possible to identify species undergoing fission in the Godiva experiments, by using the high precision TUNL data as a standard.

The Godiva critical assembly generates a neutron flux spectrum characteristic of the intrinsic ^{235}U prompt fission product neutron distribution – a distribution that can be characterized as a Watt spectrum:

$$\Phi(E) = 0.4865\sqrt{\frac{2\times(3\times10^8)^2}{939.6}}\sqrt{E}\,\sinh(\sqrt{2E})\,e^{-E}$$

The TUNL cumulative yield (CY) data in the fission neutron spectrum region were obtained at discrete neutron energies (0.58, 1.37, 2.37, and 3.6 MeV). We have weighted these discrete experimental values to reproduce the equivalent Watt energy distribution. Once this was accomplished the weighted spectra were then folded with the fission cross sections for the three relevant species (^{235}U, ^{238}U, and ^{239}Pu) to simulate their response to the Godiva Watt spectrum. This generated CY values for a "fission" neutron spectrum. The other CYs used in the fits were the TUNL high energy (i.e. 14.8 MeV) fission response for the three fissioning species of interest (^{235}U, ^{238}U, and ^{239}Pu). Table 23 presents the relevant parameters from the TUNL studies.

Table 23. Cumulative Fission yields obtained from the TUNL measurements.

	235U F CY	238U F CY	239PU F CY	235U H CY	238U H CY	239PU H CY
91Sr	5.348	4.203	2.990	4.823	3.867	2.222
92Sr	5.492	4.638	3.266	5.004	3.876	2.817
95Zr	6.114	5.138	5.161	5.174	4.891	3.924
97Zr	5.878	5.740	5.688	5.440	5.276	4.401
99Mo	5.839	6.377	6.950	5.136	5.705	4.749
103Ru	3.142	6.185	6.790	3.205	4.615	5.207
132Te	4.691	5.187	5.369	4.090	4.652	3.295
133I	6.488	6.974	7.014	5.356	5.999	4.478
140Ba	5.676	5.961	5.462	4.495	4.607	3.701
143Ce	5.479	4.725	4.466	3.815	3.908	2.803

The four Godiva data sets analyzed were from J. Burke *et al*. (^{235}U and ^{238} U) [7,8], from LANL measurements of M. Fowler [9] and National Test Site measurements from A. Tonchev [6]. The data from Refs. [6,9] were processed as raw spectral information that were fit using the PeakEasy analysis program [10] and thus are representative of the type of information that would be obtained "in field" for real nuclear forensic events. The data of J. Burke [7,8] were preprocessed and presented as CYs for specific gamma-ray transitions from multiple fission products. The four data sets were analyzed with multi-element regression analysis using the Excel "Solver" routine. The analysis was constrained with the assumption that the "unknown" observation was a combination

of the six possible "known" CY fission distributions (i.e fission spectrum or 14.8 MeV neutrons on ^{235}U, ^{238}U and ^{239}Pu). The quantitative constraints were: 1) each of the 6 possible fissioning systems had to have >= 0 yields (i.e. there could not be negative contributions from any species) and 2) the sum of the yields of the 6 components had to be equal to 1, (i.e. the 6 possible fissioning systems represented the complete universe of contributing species).

For the data sets from Refs. [6,9] no absolute fission yields were known (as would be the case in a real terrorist nuclear event) but the gamma-ray detection efficiency was known as was the gamma analysis time relative to the Godiva burst time. This allowed the spectral data to be converted into relative CYs of the specific isotopes measured. From the gamma-ray analysis of the data, error estimates were obtained for each isotope. This permitted both unweighted and weighted (by $1/\sigma^2$) analysis of each of the 4 data sets.

B. Godiva pulse-high spectra comparison

A sample of ^{235}U was irradiated with the Godiva burst reactor and four different gamma-ray spectra were recorded at time intervals relative to the Godiva burst time as shown in Table 24.

Table 24. Spectral analysis times for data sets from Ref. [6].

	T start (hr)	T stop (hr)
1st spectrum	1.439	2.439
2nd spectrum	3.439	8.439
3rd spectrum	24.439	32.439
4th spectrum	51.439	78.439

Table 25. Constrained regression analysis of Godiva data from Ref. [6].

	Unweighted Fit (with ^{135}Xe)	Unweighted Fit (no ^{135}Xe)	Weighted Fit (with ^{135}Xe)	Weighted Fit (no ^{135}Xe)
^{235}U fiss spec	0.796	0.891	1	1
^{238}U fiss spec	0	0	0	0
^{239}Pu fiss spec	0	0.051	0	0
^{235}U HE	0	0.058	0	0
^{238}U HE	0.204	0	0	0
^{239}Pu HE	0	0	0	0

Each of these spectra were analyzed to give the relative cumulative fission yields for 11 isotopes (^{91}Sr, ^{92}Sr, ^{97}Zr, ^{99}Mo, ^{105}Ru, ^{131}I, ^{132}Te, ^{133}I, ^{135}Xe, ^{140}Ba and ^{143}Ce) that overlapped with the TUNL data set. For the 135 mass chain the isotopes ^{135}I and ^{135}Xe have similar half-lives (6.97 and 9.14 hours) so a 2 component Bateman decay correction was applied to obtain the correct relative cumulative yield of the ^{135}Xe reported. Being volatile, Xe can possibly escape and introduce biases in the regression analysis. In Table 25 the unweighted and weighted constrained regression analysis parameters are presented both with and without the inclusion of the ^{135}Xe component.

All analyses correctly imply that fission spectrum neutrons on ^{235}U are the dominant reaction mechanism producing the observed isotopic distribution. The removal of ^{135}Xe in the unweighted

spectrum improves the quality of the fit. Since the uncertainties on the ^{135}Xe gamma-ray fits are relatively large, both the weighted fits with and without the ^{135}Xe component imply that the fissioning source is fission spectrum neutrons on ^{235}U.

C. Fowler data set

For the Fowler data set only one spectrum was available, consisting of a 100 minute count taken 1.6339 days after the Godiva burst irradiation of a ^{235}U sample. Again, as with the data above [6], no absolute fission yield information was available and the fitted gamma-ray peaks were corrected for detector photopeak efficiency and half-lives to obtain the relative isotopic CYs at the Godiva burst time. For the Fowler data set 10 fission product isotopes were analyzable (^{91}Sr, ^{95}Zr, ^{97}Zr, ^{99}Mo, ^{103}Ru, ^{132}Te, ^{133}I, ^{135}Xe, ^{140}Ba and ^{143}Ce). These were analyzed using the same constrained regression analysis used for the [6] data above. As with the [6] data, the ^{135}Xe was analyzed using the second order Bateman equations to correct for ^{135}I ingrowth. Additionally, the 724 keV gamma-ray line in ^{95}Zr has some interference with a similar energy line in ^{103}Ru. This was corrected by normalizing with the uncontaminated ^{95}Zr gamma-ray at 756 keV. For consistency with Ref. [6], the Fowler data [9] is also presented with and without ^{135}Xe for both weighted and unweighted analyses in Table 26.

Table 26. Constrained regression analysis of Fowler Godiva data.

	Unweighted Fit (with ^{135}Xe)	Unweighted Fit (no ^{135}Xe)	Weighted Fit (with ^{135}Xe)	Weighted Fit (no ^{135}Xe)
^{235}U fiss spec	0.972	0.971	0.377	0.530
^{238}U fiss spec	0	0	0	0.448
^{239}Pu fiss spec	0	0	0	0
^{235}U HE	0	0.029	0	0
^{238}U HE	0.028	0	0.623	0
^{239}Pu HE	0	0	0	0.022

In this case the unweighted fits with and without the ^{135}Xe contribution correctly show a dominant contribution from the fission spectrum induced fission of ^{235}U. However, the weighted fits are unsatisfactory in that fission spectrum neutrons on ^{235}U are not clearly identified as the fissioning source. Part of this inaccuracy is caused by fairly large scatter in the Fowler data set resulting in a broad, poorly constrained minimum in the least squares regression analysis.

J. Burke *et al*. performed Godiva irradiations for both ^{235}U and ^{238}U [7,8]. However, no gamma spectral information were available to us and the analysis below was done using Burke's reported values of fission product CYs for specific gamma-ray transitions in each isotope [7,8]. For consistency with the TUNL data standard we have used only J. Burke *et al*. values for the same gamma transitions as were used in the TUNL analysis. This resulted in 6 isotopes for ^{235}U that overlapped with the TUNL analysis (^{92}Sr, ^{99}Mo, ^{103}Ru, ^{132}Te, ^{140}Ba and ^{143}Ce) while 7 isotopes were available for the ^{238}U fission (^{91}Sr, ^{92}Sr, ^{95}Zr, ^{99}Mo, ^{103}Ru, ^{140}Ba, and ^{143}Ce). The J. Burke *et al*. analysis was performed with 2 gamma-ray detectors and results reported with experimental uncertainties for each. For the weighted analysis below we used the reported J. Burke *et al*. uncertainties. Since Burke did not report yields for ^{135}Xe there was no need for an analysis with and without ^{135}Xe. The constrained regression analysis of the ^{235}U J. Burke *et al*. data is presented in Table 27 and the ^{238}U values in Table 26.

Table 27. Constrained regression analysis of J. Burke *et al*. ^{235}U Godiva data [7].

	Unweighted Fit	Weighted Fit
^{235}U fiss spec	0.735	0.881
^{238}U fiss spec	0	0
^{239}Pu fiss spec	0	0
^{235}U HE	0	0.119
^{238}U HE	0.265	0
^{239}Pu HE	0	0

Table 28. Constrained regression analysis of J. Burke *et al*. ^{238}U Godiva data [8].

	Unweighted Fit	Weighted Fit
^{235}U fiss spec	0	0
^{238}U fiss spec	0.710	0.890
^{239}Pu fiss spec	0.290	0
^{235}U HE	0	0
^{238}U HE	0	0
^{239}Pu HE	0	0.110

The J. Burke data *et al*. data is the only Godiva data set that includes fission from a non ^{235}U target. It is encouraging that the regression analysis correctly identifies the predominant fission species for both the ^{235}U and ^{238}U data sets. As would be hoped for, the weighted data set gives a higher precision determination of the fissioning species than does the unweighted set.

D. Regression analysis of photon- and neutron-induced fission

Using the same regression analysis we compared the fission product yields from the same ^{240}Pu compound nucleus produced via two different fission reactions we have performed at TUNL: ^{239}Pu(n,f) and ^{240}Pu(γ,f). In the case of ^{239}Pu(n,f), an incident neutron interacts with a ^{239}Pu nucleus to produce an excited ^{240}Pu compound nucleus, which then undergoes fission. In the ^{240}Pu(γ,f) reaction, a monoenergetic photon beam interacts with ^{240}Pu nuclei, producing the same excited ^{240}Pu compound nucleus as in the ^{239}Pu(n,f) reaction [11]. In both reactions we measured the same FPYs, using the same fission chamber and gamma-ray (HPGe) counters, so that the main systematic uncertainties from both measurements are minimized.

As shown in Fig. 20, both reactions lead to the same ^{240}Pu compound nucleus. Indeed, if the incident energies of the neutron and photon beams are carefully chosen, the resulting compound nucleus has the same excitation energy in both reactions. The only difference is a spin and parity mismatch ($J^{\pi} = 0^{+},1^{+}$ from n + ^{239}Pu (for the s-wave neutrons) and $J^{\pi} = 1^{-}$ from γ + ^{240}Pu), widely believed to be inconsequential. In fact, the ^{240}Pu compound nuclei formed in neutron-induced fission and photofission are as close as one can get to this ideal scenario. Using mono-energetic photons at the HIGS facility, also located at TUNL, we excited ^{240}Pu with E_{γ}=11.2 MeV and will compare the resulting fission product yields with those obtained from neutron-induced fission on ^{239}Pu at E_{n}=0.58, 1.37, 2.4, 4.6, 9.0, and 14.8 MeV. We performed a thorough, high precision, self-consistent study that provided the most accurate experimental data on the energy dependence of the FPYs in photofission, covering the same excitation energies as in neutron-induced fission.

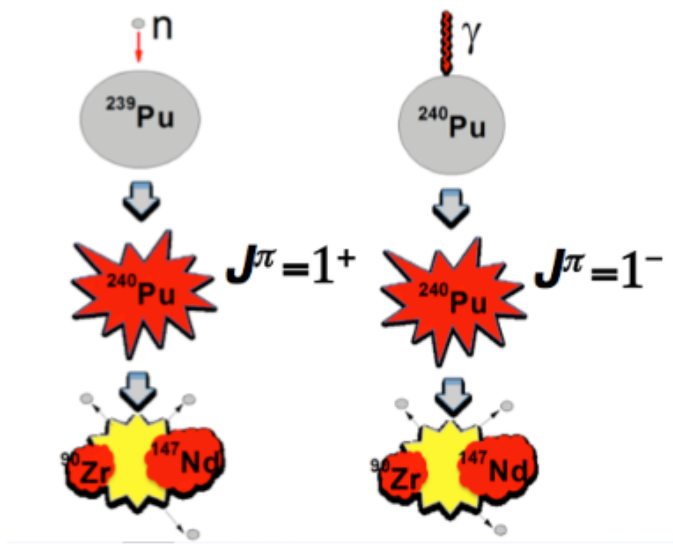

Fig. 20. *An induced fission reaction via a neutron as an incident particle used via our LLNL-LANL-TUNL collaboration, and (right) photofission reaction leading to the same compound* ^{240}*Pu nucleus. The experimental results from n+*^{239}*Pu are the same FPYs we used so far in our analysis [1].*

Table 29. Cumulative Fission yields obtained from the neutron induced fission of ^{239}Pu(n,f) at TUNL [1-5] (columns 2-7) and ^{240}Pu(γ,f) at HIGS (column 8) [11].

Isotope	E_n=0.58 MeV	E_n=1.37 MeV	E_n=2.37 MeV	E_n=3.60 MeV	E_n=4.49 MeV	E_n=14.80 MeV	E_γ=11.20 MeV
91Sr	2.78	2.89	3.19	3.16	3.08	2.62	3.176
92Sr	3.16	3.21	3.41	3.3	3.25	2.66	3.196
95Zr	4.87	5.05	5.41	5.43	5.21	4.32	4.677
97Zr	5.47	5.56	5.93	5.9	5.57	4.74	5.504
99Mo	6.79	6.95	7.11	6.87	6.73	5.42	6.494
103Ru	6.68	6.73	6.9	6.9	6.55	5.38	6.204
105Ru	5.79	5.61	5.51	5.51	5.29	4.23	4.312
127Sb	0.48	0.53	0.73	0.92	1.17	2.27	1.223
132Te	5.11	5.41	5.48	5.42	5.23	3.18	4.588
133I	6.84	6.93	7.2	7.14	6.6	4.69	6.488
135Xe	7.56	7.77	8.44	8.01	7.28	5.27	6.612
140Ba	5.49	5.38	5.52	5.52	5.23	3.95	4.436
143Ce	4.38	4.46	4.48	4.58	4.34	2.9	4.336
147Nd	2.04	2.16	2.29	2.28	2.32	1.69	3.2

As in the previous Godiva analysis seven data sets (six different incident monoenergetic neutron energies on ^{239}Pu at E_n=0.58, 1.37, 2.37, 3.60, 4.49, and 14.80 MeV and one photofission energy on ^{240}Pu at E_γ=11.20 MeV) were analyzed with multi-element regression analysis using the Excel "Solver" routine. In this analysis our photofission PYs data, which serve as a "surrogate" (or proxy) on neutron induced fission, was compared with the FPYs from the six neutron incident energies on ^{239}Pu. The question we asked is which of the neutron-induced FPYs values from these six incident neutron energies are most related to the photoinduced FPYs at 11.20 MeV? And the next question is why?

The analysis was constrained with the assumption that the probability of the 6 neutron energies had to be between 0 and 1.

Table 30. Constrained regression analysis of photofission data.

E_n=0.58 MeV	E_n=1.37 MeV	E_n=2.37 MeV	E_n=3.60 MeV	E_n=4.49 MeV	E_n=14.80 MeV
0.00	0.00	0.00	0.00	0.76	0.24

As it can be seen from Table 30 with 76% confidence level the FPYs from E_γ=11.2 MeV is correlated (or looks the same) as from E_n=4.49 MeV. Only 24% of the photofission FPYs data is correlated with the E_n=14.80 MeV FPYs data on ^{239}Pu(n,f). This is an important observation since neutron-induced fission measurements on short-lived, highly radioactive targets, such as ^{237}U(n,f)^{238}U, ^{232}U(n,f), ^{238}Pu(n,f), and ^{231}Th(n,f), could instead be replaced by photofission measurements on long-liver, near stable targets, such as ^{238}U(γ,f)^{238}U, ^{233}U(γ,f), ^{239}Pu(γ,f), and ^{232}Th(γ,f), respectively. Obviously, direct reaction such as ^{237}U(n,f)^{238}U are very difficult to perform, while indirect (surrogate or proxy) reactions like ^{238}U(γ,f)^{238}U are comparatively easy to measure. We have demonstrated this for the first time by comparison the possible relationship between the FPYs data set from two fission reactions: ^{239}Pu(n,f) and ^{240}Pu(γ,f) [12].

It should be pointed out that in the case of the FPY measurements from the ^{240}Pu(γ,f) reaction the excitation energy of ^{240}Pu compound nucleus was purposely chosen to match the excitation energy from the neutron induced fission of ^{239}Pu(n,f) at E_n = 4.49 MeV. Recall that the fission barrier of the last reaction is 6.7 MeV which combined with 4.5 MeV incident energy leads to excitation energy of about 11.2 MeV. Thus the use of regression analysis of multiple FPY data have shown the usefulness of systematic and high-precision FPYs measurements from the two most important incident particles causing fission – neutrons and photons.

Conclusions

The benefits of these analyses are the ability to: 1) determine device characteristics, 2) use the prior work of the LLNL-LANL-TUNL collaboration's highly-deferential fission product-yield experiments to determine the mean energy of the neutrons producing fission, 3) unambiguously distinguish contributions from the three main fissile materials: ^{239}Pu, ^{235}U, and ^{238}U, 4) determine the enrichment of the three fissile materials, and 5) provide early data assessment (hours to a few days) to the diagnosticians.

This approach allows the identification of the distinguishing characteristics and potential origins of collected post-detonation debris without the time or sample constraints of other methods. It uses already-identified energy-dependent fission product-yield ratios to calculate the average energy of neutrons-producing fission and provides identification of the original fissionable isotope. The proposed analysis provides a straightforward, effective approach to in-field differentiation between ^{235}U, ^{239}Pu, and the more elusive ^{238}U in unknown sample materials.

The constrained regression analysis shows promise as being a useful nuclear forensics diagnostic tool. The success of this approach vindicates the usefulness of the high precision data that has been obtained in the ongoing TUNL fission product yield program. To realize the full potential of this approach some care has to be exercised in selecting isotopes for analysis that are not volatile and that do not have interfering gamma-ray lines. Also, for cases that have isotopes in chain yields having similar half-lives, corrections for genetic decay properties must be applied.

The current TUNL data set has been optimized to analysis of fission products with half lives in the day range. This is completely appropriate for applications where fission samples are gathered in this time frame. However, for emerging nuclear forensic applications, technical advances will now make it possible to obtain gross gamma-ray spectroscopy on unseparated fission products at significantly shorter sampling times. To be able to interpret this expanded data set we wish to initiate an expanded program that will provide the same high fidelity quality fission product data that we have obtained for longer lived isotopes to those isotopes with half lives down to the minute time frame. Such an expanded data set will greatly enhance the ability and accuracy for extracting the composition and sophistication of any terrorist detonated nuclear explosion.

The current regression analysis approach has been limited to data sets obtained from Godiva irradiations. Though these are representative of a class of relevant fission data, they are not inclusive. To advance this regression analysis approach it will be very desirable to use actual fission data that has been obtained in the US nuclear testing program. With such data important issues associated with fractionation can be studied and, hopefully, used to validate an inclusive regression analysis approach.

References

[1] M. Gooden, A. Tonchev, *et al*. Nucl. Data Sheets **131,** 319 (2016).
[2] C. Bhatia, A. Tonchev, *et al*. Phys. Rev. C **91**, 064604 (2015).
[3] C. Bhatia, A. Tonchev, *et al*. Nucl. Inst. and Meth. in Phys. Research. A **757**, 7 (2014).
[4] C. Bhatia, A. Tonchev, *et al*. Nuclear Data Sheets **119** (2014) 324–327.
[5] A. Tonchev et al. Fission and Properties of Neutron-Rich Nuclei. Proceedings of the Sixth International Conference on ICFN6. p. 381 (2017).
[6] S. Stave, A. Prinke, L. Greenwood, D. Haas, J.T. Burke, J. Jo Ressler, A.P. Tonchev, W. Younes. *Reducing uncertainties for short-lived cumulative fission-product yields*. J. Radioanal. Nucl. Chem. 10.1007/s10967-015-4436-3, (2015).
[7] J.T. Burke, S. Padgett, A. Tamashiro, J.J. Ressler, G. Slavik, J. Birch, W. Younes, A. Tonchev, S. Stave, A. Prinke, L. Greenwood, B. Pierson. "Interim Report on Short-Lived Fission Product Yields from ^{235}U". September 30, 2016. LLNL-TR-704065.

[8] J.T. Burke, S.W. Padgett, A.S. Tamashiro, G. Slavik, S. Stave, A. Prinke, L. Greenwood and B. Pierson. Interim Report on Short-Lived Fission Product Yields from ^{238}U. September 15, 2017. LLNL-TR-738508.
[9] M. Fowler, Private communication.
[10] peakeasy@lanl.gov. Operated by Los Alamos National Security, LLC for the U.S. Department of Energy's National Nuclear Security Administration Inside | © Copyright 2006 Los Alamos National Security.
[11] A. Tonchev. Modernizing the fission basis. 17-LW-020 LDRD.
[12] J. Silano, A. Tonchev, et al. Manuscript prepared for publication.
[13] R.E. Marrs, E.B. Norman, J.T. Burke, R.A. Macri, H.A. Shugart, E. Browne, A.R. Smith. *"Fission-product gamma-ray line pairs sensitive to fissile material and neutron energy"*. Nuclear Instruments and Methods in Physics Research A 592 (2008) 463– 471.
[14] D.H. Beddingfield, F.E. Cecil, Nucl. Instr. and Meth. A 417 (1998) 405.
[15] T.R. England, B.F. Rider, Los Alamos National Laboratory Report LA-UR-94-3106, 1994.
[16] Nuclear Forensic Analysis. By Kenton J. Moody, Patrick M. Grant, Ian D. Hutcheon, 2015.
[17] Q. Yahua, W. Jizong, Y. Yi, Z. Ming, L. Shilong. Nucl. Instrum. and Methods. in Phys. Research. A **665**, 70 (2011).